HYDROLOGICAL PROCESSES
Hydrol. Process. **20**, 1385–1405 (2006)
Published online in Wiley InterScience (www.interscience.wiley.com). DOI: 10.1002/hyp.6098

A downscaling method of topographic index distribution for matching the scales of model application and parameter identification

N. R. Pradhan, Y. Tachikawa* and K. Takara
Disaster Prevention Research Institute, Kyoto University, Gokasho, Uji, Kyoto 611-0011, Japan

Abstract:

Higher resolution topographic information contained in the topographic index of TOPMODEL is lost when digital elevation models (DEMs) with a coarse grid resolution are used; thus, the topographic index is scale dependent, demonstrating identified model parameter values to be dependent on DEM resolution. This makes it difficult to use model parameter values identified through a different resolution of TOPMODEL. The inconsistency is the result of the difference between the scale at which the model parameters are identified and the scale at which the model is applied. To overcome this problem, scale laws that govern the relationship between the resolution of digital elevation data and geomorphometric parameters of the topographic index were analysed and a method to downscale the topographic index distribution developed to account for the difference in scales between model application and parameter identification. The method to downscale the topographic index is composed of two ideas: one involves introducing a resolution factor to account for the scale effect in upslope catchment area per unit contour length in the topographic index; the other utilizes a fractal method through steepest slope scaling to account for the scale effect on slopes. This method successfully derived a topographic index distribution of a fine-resolution DEM by using only a coarse-resolution DEM. The method has been applied successfully to the Kamishiiba catchment (210 km^2) in Japan and has demonstrated that the downscaled topographic index distribution derived using a 1000 m grid DEM is very similar to the topographic index distribution derived via fine-target-resolution DEMs. The method is then coupled with a TOPMODEL simulation to match the scales of model application and parameter identification. It is shown that the simulated runoff from the downscaled TOPMODEL applied at 1000 m resolution of the Kamishiiba catchment, with the same set of effective parameter values derived from 50 m resolution DEM, matched the simulated runoff in the 50 m DEM resolution TOPMODEL. It was also shown that TOPMODEL coupled with the downscaling method of the topographic index accurately simulated runoff for different rainfall events in the catchment without recalibration. Copyright © 2006 John Wiley & Sons, Ltd.

KEY WORDS scale invariance; downscale; fractal method; ungauged basin; topographic index; TOPMODEL

INTRODUCTION

Despite the enormous capacity of today's (and tomorrow's) information technologies, the complexity of the Earth's surface is such that the most voluminous descriptions are still only coarse generalizations of what is actually present (Goodchild, 2001). This implies that the need for continued and sustained research on scale issues is required. Since the introduction of the first blueprint of a distributed hydrological model (Freeze and Harlan, 1969), the desire to develop increasingly realistic distributed models has been spurred by requirements to improve forecasting changes in hydrological behaviour due to a variety of land use and climate change and for hydrological predictions in ungauged basins. However, in macroscale/mesoscale hydrological modelling, the concept of the aggregation approach, which assumes governing equations valid at the small scale can

* Correspondence to: Y. Tachikawa, Disaster Prevention Research Insitute, Kyoto University, Gokasho, Uji, Kyoto, Japan.
E-mail: tachikawa@flood.dpri.kyoto-u.ac.jp

Received 16 June 2004
Accepted 12 September 2005

be applied at larger scales using effective parameter values, fails because effective parameter values are scale dependent. To resolve this issue, a method that enables use of model parameters at different scales of applications is required. One method to solve the problem is to develop a scaling theory for effective model parameters with regard to modelling scales, and another is to match the scales of model application and parameter identification through introducing a scaling method for a hydrological model. This paper adopts the latter idea and discusses the method in the TOPMODEL framework.

As the spatial extent is expanded from point experiments to larger watershed regions, the direct extension of the point models requires an estimation of the distribution of model parameters and process computations over the heterogeneous land surface. If a distribution of a set of spatial variables required for a given hydrological model (e.g. surface slope, soil hydraulic conductivity) can be described using a joint density function, then digital elevation models (DEMs) and geographical information systems (GISs) may be evaluated as a tool for estimating the joint density function. The question still remains as to whether current GISs and available spatial data sets are sufficient to estimate these density functions adequately.

Several researchers (Quinn *et al*., 1991; Iorgulescu and Jordan, 1994; Wolock and Price, 1994; Zhang and Montgomery, 1994; Bruneau *et al*., 1995; Saulnier *et al*., 1997; Mendicino and Sole, 1997) have discussed the effects of DEM map scale and data resolution on the distribution of the topographic index, concluding that there is interdependence between DEM scale and topographic index distribution. Lack of methods for the translation of the scale dependence relations into effective hydrological models poses a serious problem for the ungauged basins of developing countries, where either only coarse-resolution DEM data are available or where the information gained at one scale is to be utilized in making predictions at other (usually lower) scales. The problem of transferring information gained at one scale for making predictions at a different hydrological scale is a scaling problem (Beven, 1995).

Band and Moore (1995) point out that higher frequency topographic information is lost because the larger sampling dimensions of the grids act as a filter. This is one of the fundamentals of the scale problem, and the prediction in ungauged basins becomes increasingly difficult and inaccurate without a method to resolve this issue. Thus, a downscaling/disaggregation method is needed to acquire a more realistic subgrid-scale parameterization in hydrological modelling to resolve the limitations of the aggregation method in a scale-dependent hydrological model while scaling small-scale hydrological processes and parameters to larger scales.

Analysis of physically based models such as SHE (Abbott *et al*., 1986a,b), IHDM (Rogers *et al*., 1985), and TOPMODEL (Beven and Kirkby, 1979) demonstrated that these models have, in theory, no need of preliminary calibration, since the model parameters offer clear physical meaning, which makes estimation of their values possible with regard to knowledge of the basins characteristics. However, it seems to be necessary to differentiate between 'physically based' in the sense of being based on defined assumptions and theories, and 'physically based' in the sense of being consistent with observations (Beven, 2002). A hydrological model that is physically based in theory but not consistent with observations often results from the discrepancy between the scale at which the model parameters are identified and the scale of model applications.

Even in a fully distributed physically based hydrological model, the differential equations concerning the various hydrological processes (overland flow, infiltration, percolation, etc.) are solved for single cells into which the basin is subdivided, where, by introducing a conceptualization of the phenomenon for hydrological processes, the heterogeneity of the hydrological quantities inside the cell are ignored. Conceptualizations introduced in this way result in different performances in models with variations in the assumed scale (Wood *et al*., 1988).

TOPMODEL, in practice, represents an attempt to combine the computational and parametric efficiency of a distribution function approach with the link to a physically based process description . Though it is used for a wide variety of applications, its dominating geomorphometric parameters that account for the hydrological similarity condition are also strongly influenced by the resolution of the DEM used. This results in parameter inconsistency and predictive uncertainty across scales.

In this study we focus on the influence of DEM resolution on dominating geomorphometric parameters, slope angle and upslope contributing area, which are considered as the main controls in a number of hydrological processes, and by incorporating scaling laws we developed a method to downscale the topographic index of TOPMODEL. By using this method, the topographic index distribution of a fine-resolution DEM is successfully derived by using only a coarse-resolution DEM (Pradhan *et al*., 2004). We then coupled the method to downscale the topographic index distribution with TOPMODEL to match the scales of model application and parameter identification. This allowed the use of topographic information gained at a coarser DEM scale in making hydrological predictions at a finer DEM scale.

DEPENDENCE OF TOPOGRAPHIC INDEX DISTRIBUTION ON DEM RESOLUTION

Theory of TOPMODEL

The topographic index (Kirkby, 1975) of TOPMODEL is defined as

$$\mathrm{TI} = \ln\left(\frac{a}{\tan\beta}\right) \tag{1}$$

where a is local upslope catchment area per unit contour length and β is slope angle of ground surface. In the TOPMODEL framework, the topographic index is used to distribute the local saturation deficits, given knowledge of the mean storage deficit (Beven and Kirkby, 1979; Beven, 1986, 2000a). Equation (2) shows a relationship between $\overline{S}(t)$ [L], the spatial mean storage deficit and $S(i,t)$ [L], local saturation deficit at each location i in a catchment as

$$S(i,t) = \overline{S}(t) + m\gamma - m\ln\left(\frac{a_i}{T_0\tan\beta_i}\right) \tag{2}$$

where $\tan\beta_i$ is slope angle, T_0 [$\mathrm{L^2T^{-1}}$] is the lateral (horizontal) transmissivity at zero storage deficit (i.e. when the soil is just saturated to the surface), a_i is the area draining through i per unit contour length [$\mathrm{L^2}$], m is a decay factor of saturated transmissivity of soil with respect to saturation deficit with dimensions of length [L], and γ is a constant for the basin given by

$$\gamma = \frac{1}{A}\int_A \ln\left(\frac{a_i}{T_0\tan\beta_\mathrm{i}}\right)\mathrm{d}A \tag{3}$$

According to Beven (1986, 2000a), subsurface contributions to streamflow $Q_\mathrm{b}(t)$ [$\mathrm{LT^{-1}}$] can be derived from Equation (2) as

$$Q_\mathrm{b}(t) = T_0\,\mathrm{e}^{-\lambda}\,\mathrm{e}^{-\overline{S}(t)/m} \tag{4}$$

Considering lateral transitivity to be constant in a catchment or subcatchment, the key factor for hydrologically similar conditions is the distribution function of the topographic index. Higher frequency topographic information contained in topographic indexes is lost, as the larger sampling dimensions of the grids act as a filter. This results in the hydrological similarity condition for computing the combined soil–topographic index in Equation (2) to vary accordingly with the variation in the DEM resolution used. To overcome this problem, this research has developed a method to downscale topographic index distribution.

Influence of DEM resolution on topographic index

Figure 1 shows the density function of the topographic index at four different DEM resolutions in the Kamishiiba catchment (210 $\mathrm{km^2}$) in Japan without taking into account the scale effect. A distinct shift of the topographic index density functions towards higher values is seen in Figure 1 as the resolution of the DEM becomes coarser, using the steepest slope algorithm. Saulnier *et al*. (1997) have also demonstrated a similar

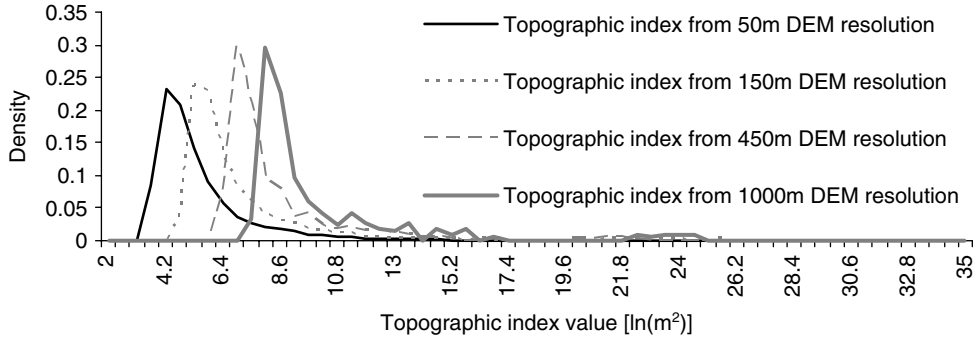

Figure 1. Effect of DEM resolution on density distribution of topographic index

Table I. DEM resolution effect on spatial mean of topographic index λ in the Kamishiiba catchment

DEM resolution (m)	50	150	450	600	1000
Spatial mean of topographic index λ ($\ln(m^2)$)	6·076	7·423	9·222	9·622	10·353

shift of topographic index density functions towards higher values as the resolution of the DEM becomes coarser when using a multi-directional algorithm (Quinn *et al*., 1995). This is a clear indication of the loss of higher frequency topographic information, as the larger sampling dimensions of the grids act as a filter. Table I shows the distinct effect of DEM resolution on the spatial mean value of the topographic index λ in Equation (5) as

$$\lambda = \frac{1}{A}\int_A \ln\left(\frac{a_i}{\tan\beta_i}\right) \mathrm{d}A \tag{5}$$

Analysing Figure 1 and Table I, we can readily conceive the error in hydrological prediction in ungauged basins using a DEM at a lower resolution when using parameter values identified at different DEM resolutions.

DEVELOPMENT OF A METHOD TO DOWNSCALE UPSLOPE CATCHMENT AREA FOR THE SOLUTION OF DEM RESOLUTION EFFECT

In a DEM-based distributed hydrological model, upslope catchment area at a point is the number of pixels draining through that point (Jenson and Domingue, 1988; Rodriguez-Iturbe and Rinaldo, 1997). In hydrological geomorphology, upslope catchment area is a key variable because of its intrinsic capability to describe the nested aggregation structure embedded in the fluvial landforms and its important physical implications (e.g. Leopold and Maddock, 1953; Rodriguez-Iturbe and Rinaldo, 1997). Most physically based models of hydrological and geomorphic processes rely on spatially distributed characterization of drainage area (e.g. Beven and Kirkby, 1979; O'Loughlin, 1986; Woods *et al*., 1997). Any upslope catchment areas smaller than the grid area of the DEM resolution used are completely lost. Thus, a portion of the upslope catchment area that can be well defined by a finer DEM resolution gets completely filtered out if that portion of the upslope catchment area is less than the grid area of the coarse-resolution DEM used.

Figure 2 shows the frequency distribution of the upslope catchment area at four different DEM resolutions in the Kamishiiba catchment (210 km^2) in Japan without taking into account the scale effect. Distinct decreases in the finer values of upslope catchment area are observed in Figure 2 when the resolution of DEM becomes coarser. In Figure 2, the smaller upslope catchment areas less than 1 km^2 that appear in over 97% of the catchment in 50 m DEM resolution are completely lost when switched to a 1000 m DEM resolution. Figure 3

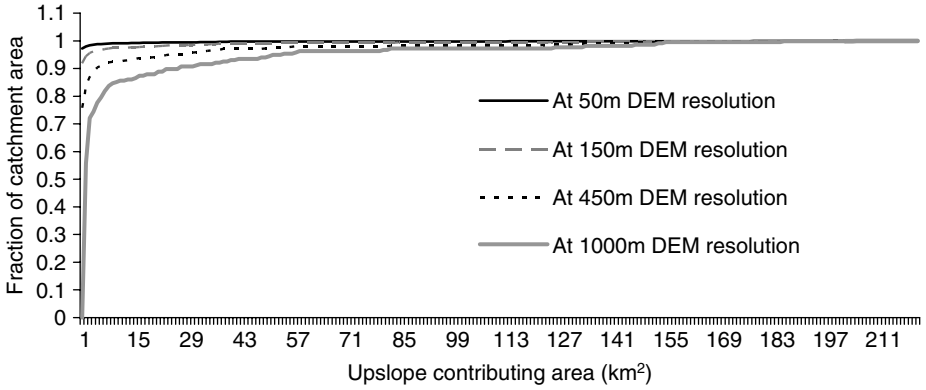

Figure 2. Comparison of distribution functions of upslope catchment area obtained from different DEM resolutions in the Kamishiiba catchment (210 km^2)

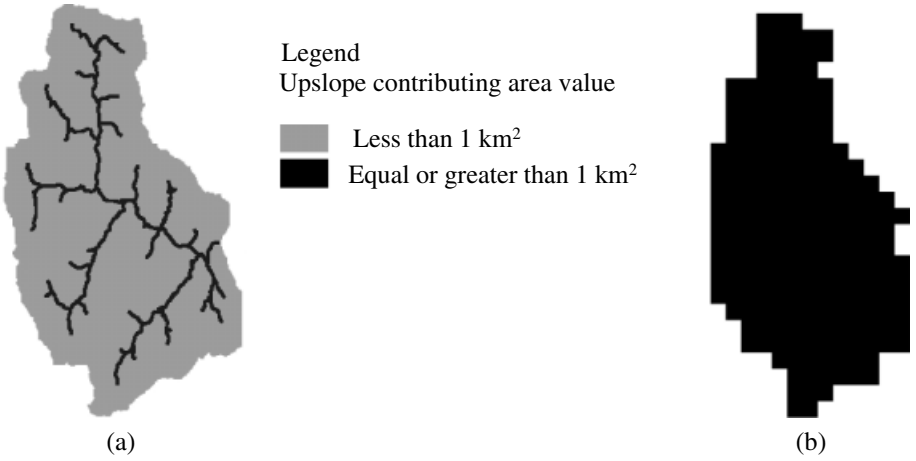

Figure 3. Comparison of upslope catchment area from (a) 50 m DEM resolution and (b) 1000 m DEM resolution in the Kamishiiba catchment (210 km^2)

further clarifies this fact. Figure 3a shows that, at 50 m DEM resolution, most of the catchment is displayed as possessing upslope catchment area of less than 1 km^2, whereas Figure 3b shows that, at 1000 m DEM resolution, there is no grid having an upslope catchment area less than 1 km^2.

In fact, the smallest upslope catchment area derived from a DEM resolution is a single grid of the DEM at that resolution. From this point of view, we introduced the total number of sub-grids N_s within a coarse-resolution grid (see Figure 4) to derive scaled upslope catchment area as

$$C_{i,\ \mathrm{scaled}} = \frac{C_i}{N_s I_f} \tag{6}$$

where the suffix i is a location in a catchment, $C_{i,\ \mathrm{scaled}}$ is the scaled upslope catchment area at a point I, and I_f is introduced as an influence factor.

Figure 2 shows that, as the upslope catchment area increases, the distributions of the upslope catchment area values given by coarse- and fine-resolution DEMs converge; thus, the influence of N_s on C_i must gradually decrease in Equation (6) as C_i becomes larger. For this reason we introduced influence factor I_f in Equation (6). From the discussion of influence of N_s on C_i, the following three points are proposed:

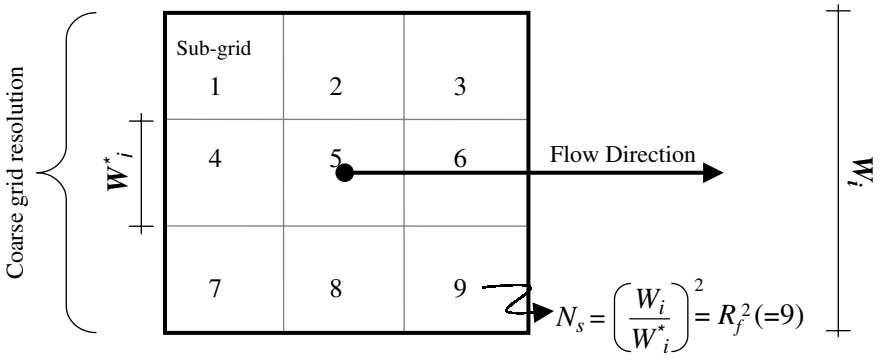

Figure 4. Concept of N_s as number of sub-grids within a coarse grid resolution

1. At the catchment divide portion where the upslope catchment area in a coarse-resolution DEM is a single coarse-resolution grid area, the value of the influence factor I_f in Equation (6) is equal to unity, demonstrating that N_s has complete influence on C_i.
2. Considering the upslope catchment area given by a coarse-resolution DEM and target fine-resolution DEM are equal at the outlet of the catchment, the value of influence factor I_f in Equation (6) is equal to $1/N_s$, showing that N_s has no influence on C_i.
3. Exponential decay of the influence factor is taken from the value 1 defined in point 1. to $1/N_s$ defined in point 2. as the upslope catchment area increases. Thus, I_f is defined as

$$I_f = e^{[(1-N_i)H]/N_o} \tag{7}$$

where N_i is the number of coarse-resolution grids contained in the upslope catchment area at a location i in the catchment and N_o is the number of coarse-resolution grids contained in the upslope catchment area at the outlet of the catchment. H in Equation (7) is introduced as a parameter to define the variation in the influence factor as a function of N_o and N_s. Considering the influence of N_s on C_i in Equation (6) is almost negligible at the outlet of the catchment, where $N_i = N_o$ and $I_f = 1/N_s$, the value of H can be obtained from Equation (7) by substituting $N_i = N_o$ and $I_f = 1/N_s$ as

$$H = \frac{N_o}{N_o - 1} \ln N_s \tag{8}$$

Finally, we developed a method to downscale the upslope catchment area from Equations (6) and (7) as

$$C_{i,\ \text{scaled}} = \frac{C_i}{N_s\ e^{[(1-N_i)H]/N_o}} \tag{9}$$

The analysis and derivation of downscaling method of upslope catchment area was developed from the assumption that upslope catchment area at a point is the number of pixels draining through that point. Although the multiple flow-direction approach is an approximate form of subgrid-scale flow pathway interpolation (Quinn *et al.*, 1991), it is also affected by the loss of information of finer resolution upslope catchment area when using coarse-resolution DEMs. This is because the values of distributed upslope catchment area at the catchment divide, according to weighted percentages relative to the value assumed by the slope, are higher in a coarse grid cell than in a fine grid cell.

The method to downscale the upslope catchment area is applied to the Kamishiiba catchment (210 km^2). Using Equation (9), the upslope catchment area is downscaled from 1000 m DEM resolution to various DEM grid resolutions as shown in Figure 5. In contrast to Figure 2, Figure 5a–d shows that the distributions of

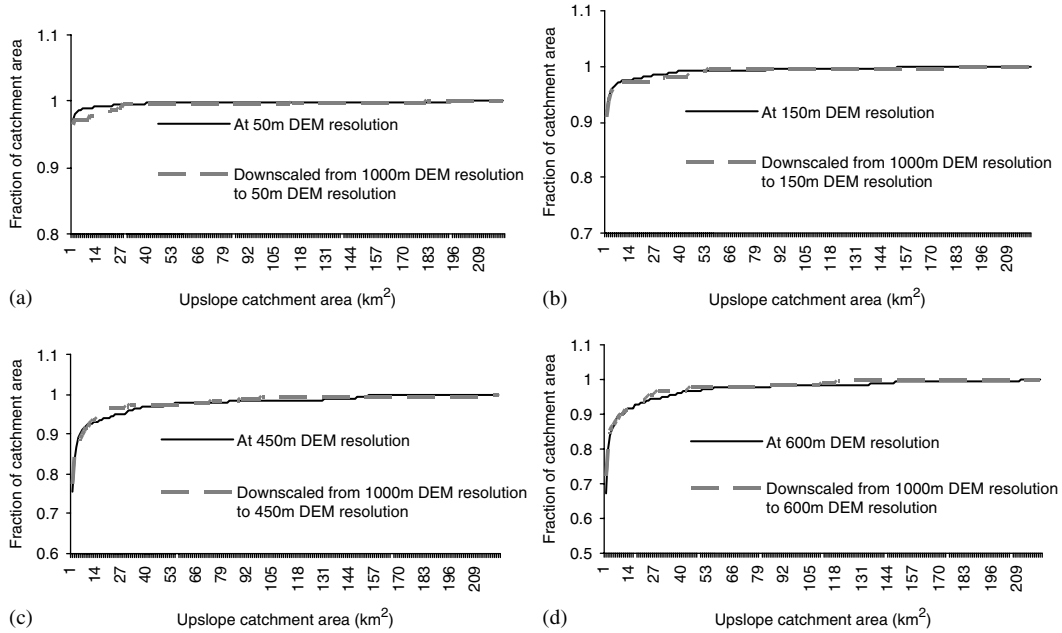

Figure 5. Comparison of distribution function of upslope catchment area from a 1000 m grid-resolution DEM to a finer grid-resolution DEM and the distribution function of the upslope catchment area at the fine scale in the Kamishiiba catchment (210 km^2). (a), (b), (c) and (d) are the comparisons for 50 m, 150 m, 450 m and 600 m grid resolutions respectively

upslope catchment area from 50, 150, 450 and 600 m DEM resolutions match the distribution of downscaled upslope catchment area from 1000 m DEM resolution to the respective DEM resolution. This shows that the proposed method to downscale the upslope catchment area given by Equation (9) can be successfully used to obtain higher resolution assessments of upslope catchment area at finer grid sizes by using only a coarse DEM resolution.

DEVELOPMENT OF THE METHOD TO DOWNSCALE TOPOGRAPHIC INDEX OF TOPMODEL

As topographic index is scale dependent, this results in identified parameter values being dependent on the DEM resolution. This makes it difficult to use model parameter values identified in a model of different resolution. To overcome the problem, a scale-invariant model of topographic index is proposed. A resolution factor and a scaled slope with a fractal method is introduced in the scale-invariant model of the topographic index distribution to scale upslope catchment area per unit contour length a and slope angle of the ground surface β.

Resolution factor in topographic index

Figure 1 shows that higher frequency topographic information contained in the topographic index distribution is lost. One of the main reasons for the movement of the topographic index distribution towards higher values while using coarse-resolution DEMs is due to the filtering of the upslope catchment area defined by a fine DEM resolution, as explained previously. To obtain the lost portion of the upslope catchment area defined by a target fine-resolution DEM, we introduced scaled upslope catchment area, as explained in Equation (6), to the topographic index, as shown in Equation (10). In the TOPMODEL framework, the conceptual derivation of contour length by a single flow-direction approach or multiple flow-direction approach overestimates the contour length at the catchment divide portion when a coarse DEM is used. Thus, to achieve the unit contour

length at the target subgrid scale, the unit contour length at the available coarse-resolution DEM is divided by the resolution factor R_f in Equation (10) as

$$\mathrm{TI} = \ln\left[\frac{\dfrac{C_i}{N_s I_f}}{\left(\dfrac{W_i}{R_f}\right)\tan\beta_i}\right] \tag{10}$$

where TI is the topographic index, C_i is the upslope catchment area of the coarse-resolution DEM, W_i is the unit contour length at the available coarse-resolution DEM (see Figure 4), N_s is the total number of subgrids within a coarse-resolution grid (see Figure 4), and i is a location in a catchment. Resolution factor R_f in Equation (10) is defined as

$$R_f = \frac{\text{Coarse DEM Resolution}}{\text{Target DEM Resolution}} = \frac{W_i}{W_i^*} \tag{11}$$

where W_i^* is the unit contour length of the target DEM resolution (see Figure 4). It is clear from Figure 4 that

$$N_s = R_f^2 \tag{12}$$

From Equations (10) and (12), the resolution factor is introduced in the topographic index as

$$\mathrm{TI} = \ln\left(\frac{C_i}{W_i R_f \tan\beta_i}\right) - \ln I_f \tag{13}$$

Fractal method for scaled steepest slope

Figure 6 shows the frequency distribution of the steepest slope at four different DEM resolutions in the Kamishiiba catchment (210 km^2) in Japan without taking into account the scale effect. Figure 6 clearly shows that slopes derived from DEMs vary with the spatial resolution, with values decreasing at larger pixel sizes. The underestimation of slopes when using the coarse-resolution DEMs can seriously affect the accuracy of hydrological and geomorphological models (Zhang *et al*., 1999). To scale the local slope, we followed the fractal theory in topography and slope proposed by Klinkenberg and Goodchild (1992) and Zhang *et al*. (1999) and developed a modified fractal method for steepest slope.

Fractal method for average slope estimation proposed by Zhang et al. (1999). The variogram technique is used to calculate the fractal dimension in a region when the logarithm of the distance between samples

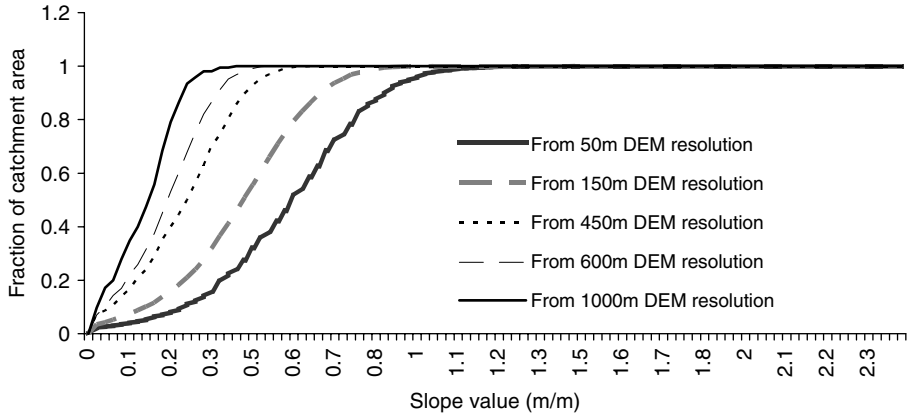

Figure 6. Comparison of steepest slope distribution function obtained from different DEM resolutions in the Kamishiiba catchment (210 km^2)

is regressed against the logarithm of the mean squared difference in the elevations for that distance. The variogram equation used by Klinkenberg and Goodchild (1992) to calculate the fractal dimension of topography is

$$(Z_p - Z_q)^2 = k d_{pq}^{4-2D} \tag{14}$$

where Z_p and Z_q are the elevations at points p and q, d_{pq} is the distance between p and q, k is a constant, and D is the fractal dimension. The topographic fractal properties of Equation (14) can be used to scale slope as follows:

$$\frac{Z_p - Z_q}{d_{pq}} = \alpha d_{pq}^{1-D} \tag{15}$$

where $\alpha = \pm k^{0.5}$ is a constant. Because the left part of Equation (15) represents the surface slope, it can be assumed that the slope value θ is associated with its corresponding grid size d by the equation

$$\theta = \alpha d^{1-D} \tag{16}$$

This implies that slope will be a function of the measurement scale if the topography is unifractal in a specified range of measurement scale (Zhang *et al*., 1999). However, it is impossible to predict the spatial patterns of slopes due to the single value of the fractal dimension and the coefficient in the fractal slope equation for the whole DEM. To overcome this problem, Zhang *et al*. (1999) proposed that the coefficient α and fractal dimension D of Equation (16) are mainly controlled by the standard deviation of the elevation of the sub-regions in a DEM and derived the regressed relations between α and D separately with the standard deviation of the elevation. In deriving the regressed relation, Zhang *et al*. (1999) considered the smallest sub-area (window) to be composed of 3×3 pixels. Hence, elevations of nine neighbouring grids in the DEM were taken to obtain the standard deviation of the elevation for a sub-area.

We found that the slope derived from the method by Zhang *et al*. (1999) tends to match only with the average slope within the 3×3 moving-window pixels of the coarse-resolution DEM, but completely failed to take into consideration the steepest slope defined as the direction of the maximum drop from centre pixel to its eight nearest neighbours, known as the D8 method. Thus, we propose a modified fractal method for the steepest slope.

Fractal method for steepest slope. A modified model for the fractal method to account for the steepest slope change due to change in DEM resolution is described as follows:

1. Unlike the distance d in Equation (16) being represented by constant grid size, this distance d in every grid point in a 3×3 pixels moving window is provided as the steepest slope distance d_{steepest}. Figure 7a shows the steepest slope distance d_{steepest} to be $\mathrm{d}x$, $\mathrm{d}y$ and $\sqrt{\mathrm{d}x^2 + \mathrm{d}y^2}$ according to the direction of steepest descent of the slope in the X-axis, Y-axis and diagonal axis DD respectively.
2. It is found that there is not much variation in standard deviation of elevation from a high-resolution DEM to a low-resolution DEM in the same sub-area. Fractal dimension D is related to the standard deviation of elevation σ (m) in a 3×3 pixels moving window as per Zhang *et al*. (1999).

$$D = 1{\cdot}135\,89 + 0{\cdot}084\,52 \ln \sigma \tag{17}$$

3. The fluctuations of the coefficient α values in Equation (16) over different locations were found to be higher in comparison with the D value. Unlike the method by Zhang *et al*. (1999), in which α values are derived from standard deviation σ of the elevation in 3×3 pixels moving window, we developed a new method where the coefficient α values are derived directly from the steepest slope of the available coarse-resolution DEM, while maintaining that the steepest slope itself represents an extreme fluctuation. The modified equation is

$$\theta_{\text{steepest}} = \alpha_{\text{steepest}} d_{\text{steepest}}^{1-D} \tag{18}$$

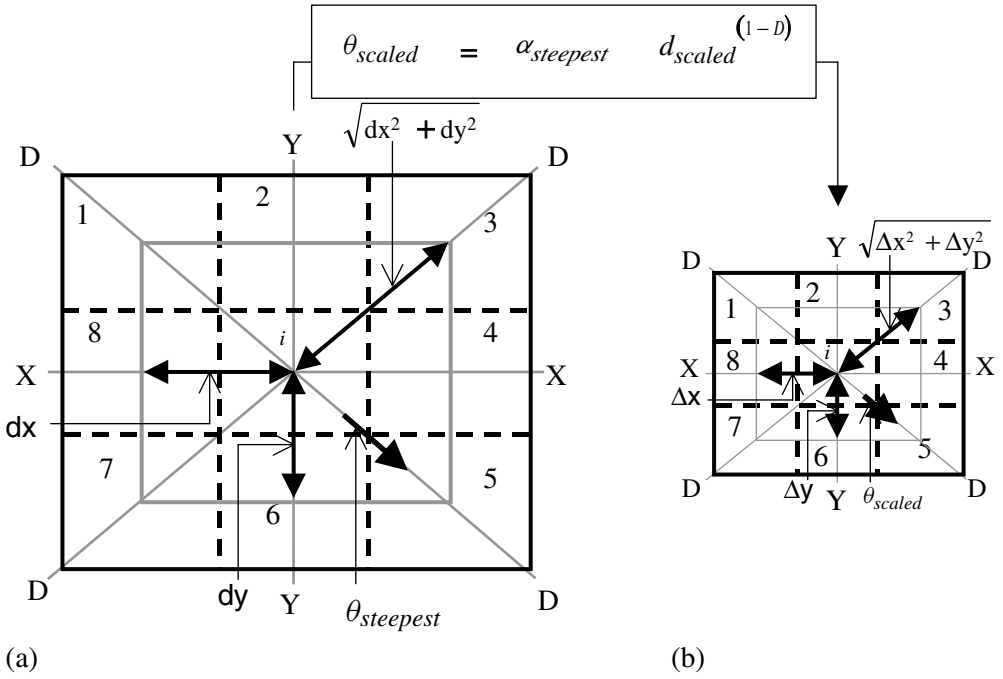

Figure 7. Fractal method for scaled steepest slope at a location i of the 3×3 pixels moving window: (a) steepest slope structure of the available coarse-resolution DEM; (b) scaled steepest slope structure of the target resolution DEM

In Figure 7a for example, where the steepest slope is shown in diagonal direction, α_{steepest} at that location i from Equation (18) is given by

$$\alpha_{\text{steepest}} = \frac{\theta_{\text{steepest}}}{(\sqrt{dx^2 + dy^2})^{1-D}} \tag{19}$$

where dx and dy are the grid sizes in the X-axis and Y-axis respectively and θ_{steepest} is the steepest slope using the coarse-resolution DEM.

4. While downscaling, the distance variation in the target resolution DEM is defined according to the direction of the steepest slope in the coarse-resolution DEM. Hence, in Figure 7b the downscaled steepest slope θ_{scaled} is shown to be in the same direction as that of the coarse-resolution DEM steepest slope (Figure 7a). Thus, in Figure 7b, the downscaled steepest slope θ_{scaled} is given as

$$\theta_{\text{scaled}} = \alpha_{\text{steepest}} d_{\text{scaled}}^{1-D} \tag{20}$$

where $d_{\text{scaled}} = \sqrt{\Delta x^2 + \Delta y^2}$ in Figure 7b and Δx, Δy are the grid sizes of the target resolution DEM in the X-axis and Y-axis respectively. Thus, using the coarse-grid DEM for each grid, the value of D is obtained from Equation (17) and α_{steepest} is obtained from Equation (19). Then, by using Equation (20), the downscaled steepest slope θ_{scaled} is obtained by defining the distance d_{scaled} at target DEMs.

Figure 8a–d shows the comparison of scaled slope distribution function from the 1000 m grid-resolution DEM to the 600 m, 450 m, 150 m and 50 m grid-resolution DEMs by using Equation (20) and the distribution function of the slope at those respective fine-scale DEMs. A close fit of the frequency distribution of the scaled slope from the 1000 m grid-resolution DEM to 600 m, 450 m, 150 m grid-resolution DEMs is shown in Figure 8a–c, and Figure 8d demonstrates that Equation (20) overestimated the slope when downscaling from

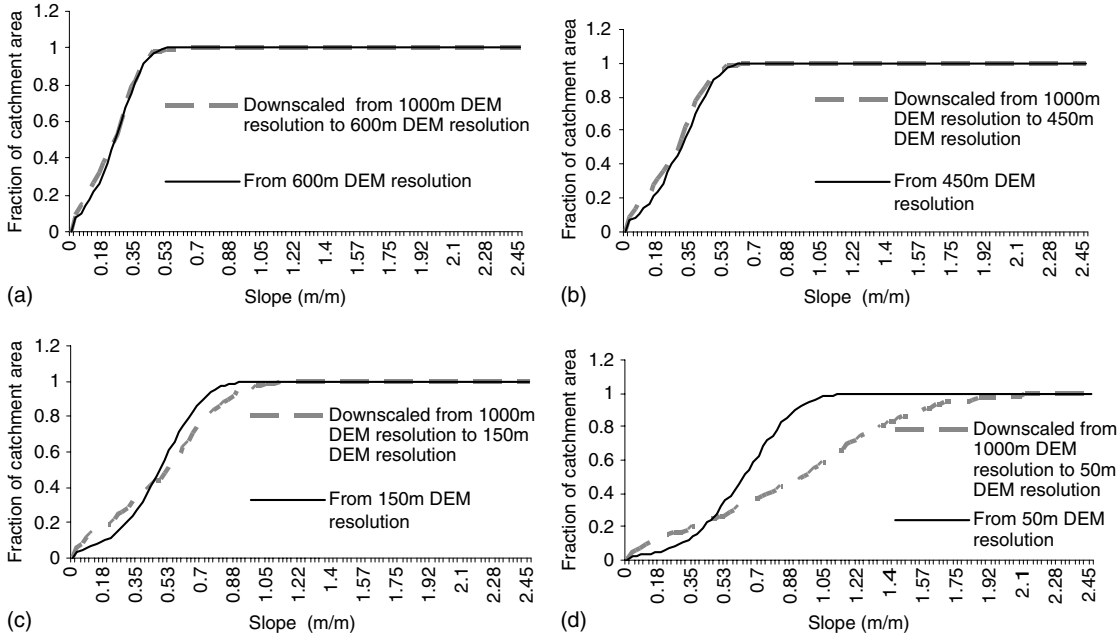

Figure 8. Comparison of distribution function of scaled steepest slope from a 1000 m grid-resolution DEM to a finer grid-resolution DEM and the frequency distribution of the steepest slope at the fine scale in the Kamishiiba catchment (210 km^2). (a), (b), (c) and (d) are the comparisons for 600 m, 450 m, 150 m and 50 m grid resolutions respectively

1000 m to 50 m DEM resolution. This causes the downscaled topographic index distribution from 1000 m to 50 m DEM resolution to shift slightly below that of the original 50 m DEM resolution topographic index distribution. In Equation (20), slope is a function of the measurement scale by assuming that topography is unifractal in a specified range of measurement scale. This unifractal concept can break down at very fine scales (Andrle and Abrahams, 1989; Klinkenberg and Goodchild, 1992). This possible break in the unifractal condition at fine scales and its possible solution method is for further research work. In this study we assume that the lower applicable limit of Equation (20) is 150 m when downscaling the slope distribution from a 1000 m grid resolution to lower grid-resolution DEMs. Thus, when downscaling slope distribution from 1000 m to 50 m DEM resolution, the slope is downscaled to 150 m, and the distribution is used for downscaling to 50 m.

Scaled topographic index distribution

By combining Equations (13) and (20), the method to downscale the topographic index is defined as

$$\mathrm{TI}_{\mathrm{scaled}} = \ln\left(\frac{C_i}{W_i R_{\mathrm{f}} \theta_{\mathrm{scaled}}}\right) - \ln I_{\mathrm{f}} \tag{21}$$

The scaled topographic index $\mathrm{TI}_{\mathrm{scaled}}$ includes the resolution factor to account for the effect of scale on upslope catchment area per unit contour length and the fractal method for scaled steepest slope as an approach to account for the effect of scale on slope.

COUPLING SCALE-INVARIANT TOPOGRAPHIC INDEX DISTRIBUTION IN THE TOPMODEL FRAMEWORK

Total runoff is calculated as the sum of two flow components: saturation excess overland flow from variable contributing areas (Dunne and Black, 1970) and subsurface flow from the saturated zone of the soil, as shown

in Figure 9. Areas with $S(i, t) \leq 0$ (in Equation (2)) are contributing areas for saturation excess overland flow. Following Equations (2), (3) and (5), the dependency of $S(i,t)$ on other variables is shown as

$$S(i, t) = f(\overline{S}(t), T_0, \lambda, m, \mathrm{TI}) \tag{22}$$

Again, from Equation (4), the dependency of subsurface flow from the saturated zone (S_Z [L] in Figure 9), $Q_b(t)$ is written as

$$Q_b(t) = g(\overline{S}(t), T_0, \lambda, m) \tag{23}$$

In Equations (22) and (23), the only observable independent variable accounting for heterogeneity is the topographic index TI. The parameters T_0, λ, m and $\overline{S}(t)$ in the catchment or subcatchment are directly influenced by the topographic index value, which changes with the resolution of the DEM used. This makes recalibration in the model compulsory when the scale of application of the model differs from the scale at which the model parameters are identified. Thus, in the TOPMODEL concept, to make the topographic index value scale invariant, Equation (1) has been replaced by Equation (21). The scale invariant-function defined by Equation (21) is $\overline{S}(0)$ based on scale laws and does not add any extra parameter burden when coupled with TOPMODEL.

Root zone store R_Z [L] in Figure 9 for each topographic index value is depleted only by evapotranspiration, and that water is added to the unsaturated zone drainage storage U_Z [L] only after the root zone reaches field capacity or maximum root zone storage $R_{Z\max}$ [L]. The drainage from the unsaturated zone is assumed to be essentially vertical and drainage flux per unit area q_v [LT^{-1}] is calculated for each topographic index class (Beven, 1986) as

$$q_v\ (i, t)\Delta t = \min\{T_0\ \mathrm{e}^{-S(i,t)/m}\ \Delta t, U_Z(i, t)\} \tag{24}$$

where Δt [T] is calculation time step. The initial condition for average saturation deficit is derived from Equation (4) taking $Q_b(0)$ as the initial observed discharge (Beven, 1987). $\overline{S}$ in the successive time step is calculated by

$$\overline{S}(t + 1) = \overline{S}(t) - Q_v(t)\Delta t + Q_b(t)\Delta t \tag{25}$$

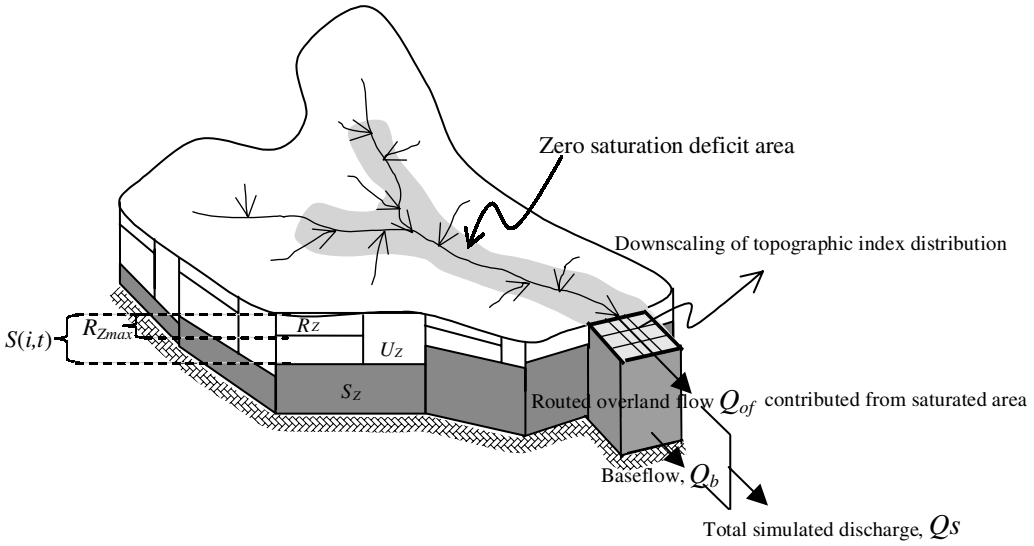

Figure 9. Coupling the method to downscale topographic index distribution in the TOPMODEL framework

where $Q_v(t)$, the total input to groundwater from the unsaturated zone, is the sum of $q_v(t)$ over all grids in the catchment, and $Q_b(t)$ is the groundwater discharge to the stream. The Muskingum-Cunge routing method is used for calculating hill slope channel routing (Cunge, 1969).

RESULTS AND DISCUSSION

Application of the method to downscale the topographic index distribution

The method to downscale the topographic index of TOPMODEL is applied to the Kamishiiba catchment (210 km^2) in Japan. Using Equation (21), the topographic index is then downscaled. Figure 10 shows the comparison of the downscaled topographic index distribution function using Equation (21) from 1000 m to 50 m DEM resolution with variable I_f given by Equation (7) and with constant $I_f = 1$. In Figure 10, no significant change is seen in the topographic index distribution, except for the highest topographic index values in the lowest density range in a catchment. This is because I_f values from Equation (7) are also almost equal to unity at the higher density distribution of topographic index values. This is why, for the rest of the analysis in this discussion, $I_f = 1$ is assumed in Equation (21). This is the same as taking only the first term in Equation (13). Moreover, in the TOPMODEL framework, the conceptual derivation of contour length by the single flow-direction approach or the multiple flow-direction approach underestimates the contour length at the catchment outlet when a fine DEM resolution is used. Also, the introduction of I_f with R_f and W_i in Equation (10) can correct this error by varying the contour length derivation from the target fine grid resolution at the catchment divide portion to the available coarse grid resolution at the catchment outlet portion. The introduction of I_f with R_f in Equation (10) is also the same as taking only the first term in the right hand side of Equation (13).

Table II shows the scaled topographic constant λ from a 1000 m grid-resolution DEM to various target DEM resolutions by applying the downscaling method. The downscaled values of λ from 1000 m grid resolution to finer DEM resolutions in Table II are almost equal to the values of λ in Table I derived from those fine grid-resolution DEMs.

Figure 11a is the topographic index distribution using a 1000 m DEM. Figure 11b–e shows the scaled topographic index distribution obtained by using the downscaling method with the same 1000 m grid-resolution DEM to the 600 m, 450 m, 150 m and 50 m grid-resolution DEMs respectively. Figure 11f is the topographic index distribution using the 50 m DEM. Distinct differences can be seen between the spatial distribution of the topographic index in Figure 11a and Figure 11f for the 1000 m grid-resolution DEM and the

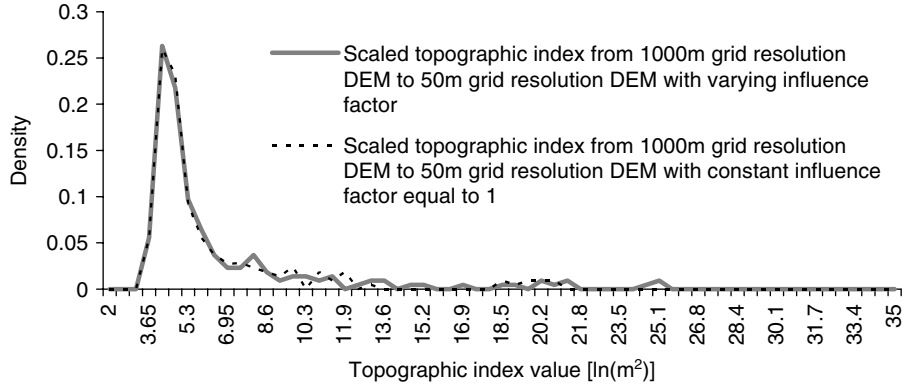

Figure 10. Effect of influence factor on scaled topographic index distribution. Comparison of density function of scaled topographic index using Equation (21) with varying influence factor given by Equation (7) and with constant influence factor equal to unity. In both cases the downscaling is made from a 1000 m to a 50 m grid-resolution DEM

Table II. Spatial mean of topographic index λ using downscaled topographic index for target resolutions derived from 1000 m grid DEM in the Kamishiiba catchment

Target DEM resolution (m)	50	150	450	600
Spatial mean of topographic index λ (ln(m^2))	6·474	7·573	9·110	9·604

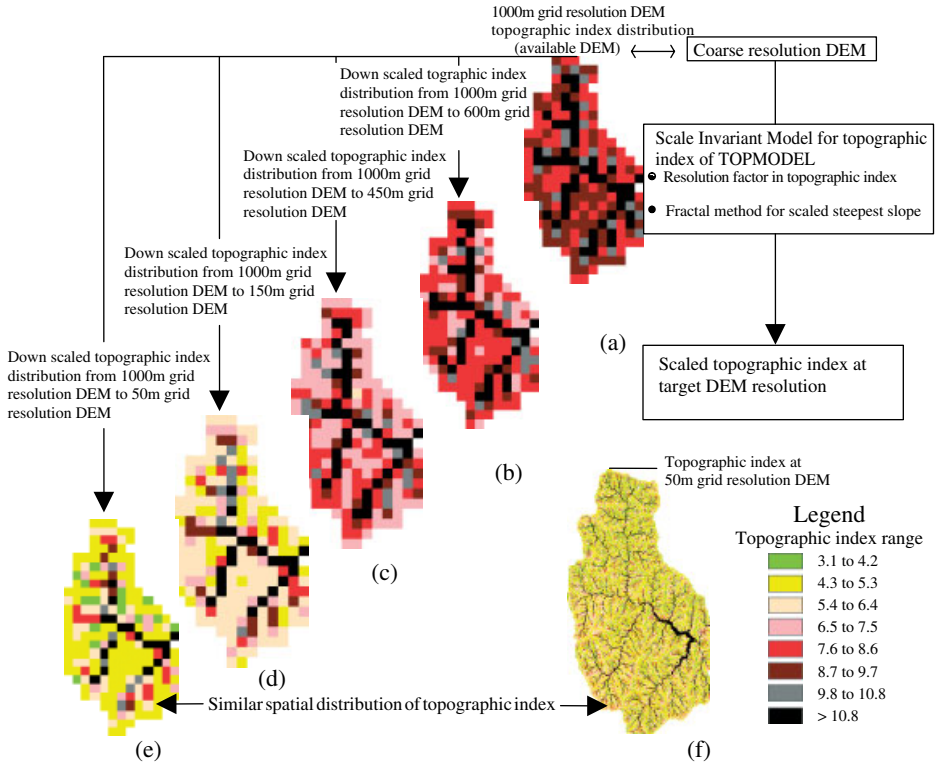

Figure 11. Spatial distribution of scaled topographic index applied to the Kamishiiba catchment (210 km^2). (a) Topographic index distribution using a 1000 m DEM resolution. (b), (c), (d) and (e) Scaled topographic index distributions obtained from a 1000 m DEM resolution to 600 m, 450 m, 150 m and 50 m DEM resolutions respectively. (f) Topographic index distribution using a 50 m DEM resolution

50 m grid resolution DEM respectively. The spatial distribution of topographic index displayed in Figure 11e matches with the existing reality displayed in Figure 11f.

Figure 12a–d shows the comparison of scaled topographic index distribution from the 1000 m grid-resolution DEM to the 50 m, 150 m, 450 m and 600 m grid-resolution DEMs by using the downscaling method and the density function of the topographic index at a different finer scale. A close fit of density functions of scaled topographic indices from the 1000 m grid-resolution DEM to various grid-resolution DEMs is shown in Figure 12. The proposed method pursues a framework for downscaling the topographic index distribution from a coarse resolution to a specific fine-resolution DEM to obtain higher resolution topographic information. Obtaining the specific fine-resolution DEM that is most suitable for a hydrological model is not within the scope of this paper. Zhang and Montgomery (1994) suggest from their analysis that, for many landscapes, a 10 m grid size presents a rational compromise between increasing resolution and data volume required for simulating geomorphic and hydrological processes. Quinn *et al*. (1991) demonstrated

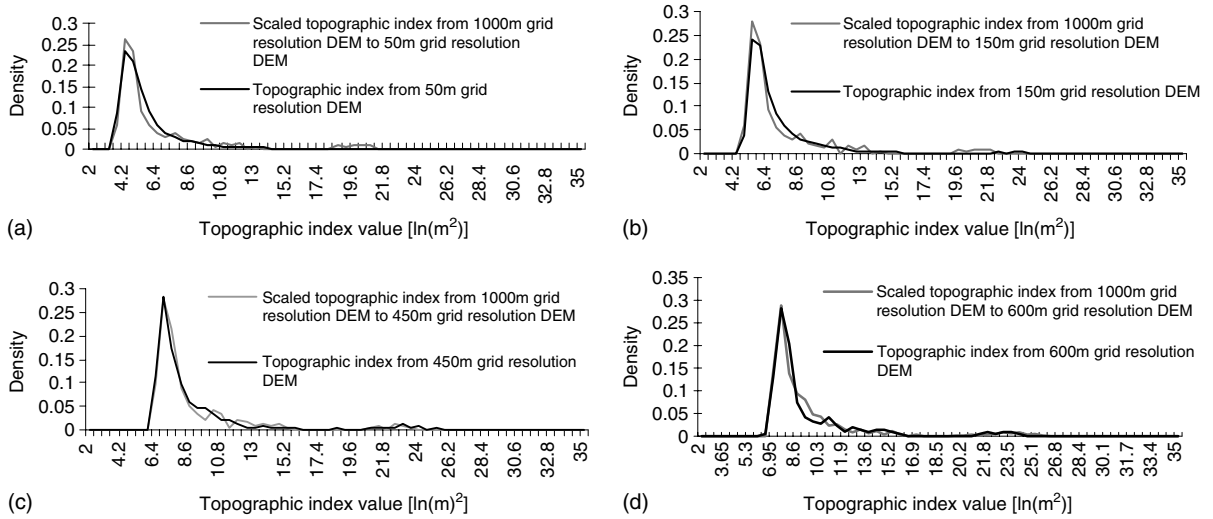

Figure 12. Comparison of density function of scaled topographic index from a 1000 m grid-resolution DEM to a finer grid-resolution DEM and the density function of the topographic index at the fine scale in the Kamishiiba catchment (210 km^2). (a), (b), (c) and (d) are the comparisons for 50 m, 150 m, 450 m and 600 m grid resolutions respectively

that features of much less than 50 m resolution are significant in hydrological routing. It is hoped that this study can be further extended to develop the downscaling method to 10 m DEM resolution and finer.

Analysis of prediction error when the parameter identification scale and model application scale are mismatched

Figure 13 shows three different rainfall events, Event(1), Event(2) and Event(3), in the Kamishiiba catchment (210 km^2). In Figure 13, A(1), A(2) and A(3) are the simulation results using a 50 m DEM resolution TOPMODEL; B(1), B(2) and B(3) are the simulation results using a 1000 m DEM resolution TOPMODEL; C(1), C(2) and C(3) are the simulation results from TOPMODEL by coupling the downscaling method of topographic index distribution, applied at 1000 m DEM resolution and the topographic index downscaled to 50 m DEM resolution. The labels (1), (2) and (3) denote the simulation results that belong to rainfall Event(1), Event(2) and Event(3) respectively.

For all the simulation results shown in Figure 13, the effective parameters of TOPMODEL are identified by the 50 m DEM resolution TOPMODEL, as shown in Table III. Although the effective parameters identified in Table III are calibrated by the 50 m DEM resolution TOPMODEL in Event(2) as shown for A(2) in Figure 13, resulting in a Nash efficiency of 94%, consideration is also given to the model consistency when applying the 50 m DEM resolution TOPMODEL with the same set of parameters to other events. In Event(1) and Event (3) the Nash efficiencies are 90% and 78% respectively, as shown in Figure 13. In accordance with the work of Ambroise *et al*. (1996) and Güntner *et al*. (1999), a parameter value for m was derived from the first-order hyperbolic function that fitted the recession curve obtained from the observed discharge of rainfall Event(1). The value of the parameter m derived by the recession analysis is 0·07 m, which is found to be equal to the calibrated parameter value of m by the 50 m DEM resolution TOPMODEL.

Comparing B(1), B(2), and B(3) with A(1), A(2), and A(3) respectively in Figure 13, it is seen that the magnitudes of the differences in TOPMODEL predictions based on different DEM resolutions are significant when the same set of parameter values are used. The simulated discharges for B(1), B(2) and B(3) in Figure 13 are very sensitive to rainfall, showing overestimation of discharge in the rainfall duration and underestimation of discharge as soon as the rainfall stopped or diminished. Because of this inconsistency in the 1000 m DEM

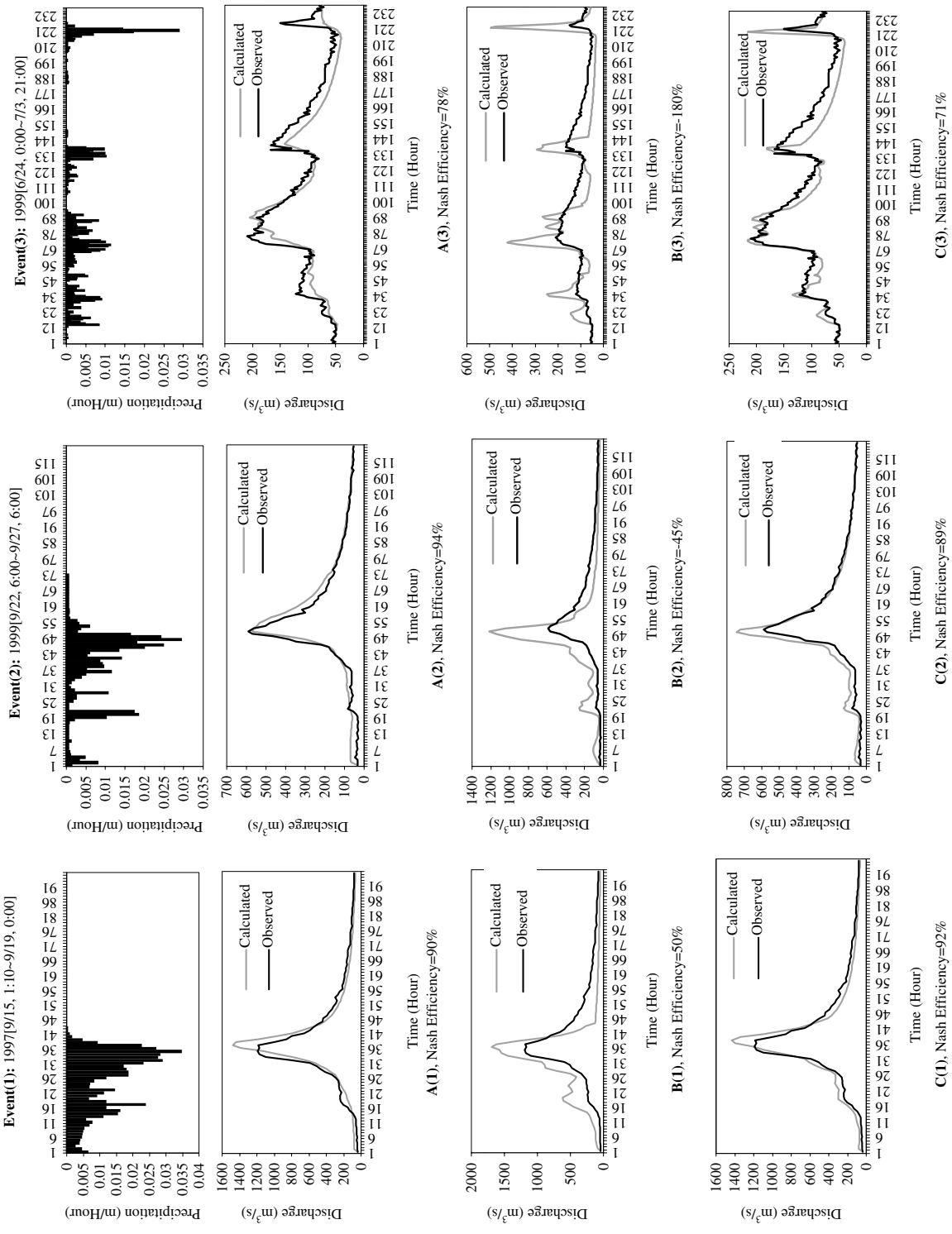

Figure 13. Simulation results of TOPMODEL (with and without coupling the downscaling method of topographic index) applied to the Kamishiiba catchment (210 km^2). A(1), A(2), A(3) are the simulation results from a 50 m DEM TOPMODEL. B(1), B(2), B(3) are the simulation results from a 1000 m DEM TOPMODEL without scale-invariant model for topographic index. C(1), C(2), C(3) are the simulation results from TOPMODEL at a 1000 m DEM resolution and topographic index downscaled to a 50 m DEM resolution. The same set of effective parameter values, identified by a 50 m DEM resolution TOPMODEL using Event(2), is used for all the simulation results in A(1), A(3), B(1), B(2), B(3), C(1), C(2) and C(3)

Table III. Effective parameter values identified by a 50 m DEM resolution TOPMODEL for Event(2) used for different events and different DEM resolution TOPMODELs in the Kamishiiba catchment

T_0 (m^2 h^{-1})	m (m)	R_{Zmax} (m)
9·8	0·07	0·001

resolution TOPMODEL prediction, the Nash efficiencies for B(1), B(2), and B(3) in Figure 13 decreased drastically to 50%, −45% and −180% respectively when retaining the same parameter values identified for the 50 m DEM resolution TOPMODEL.

Earlier, in Table I, we showed that, as the resolution of DEMs is coarsened, the spatial mean value of topographic index λ in Equation (5) increases. As λ increases, the initial average saturation deficit derived from Equation (4) decreases. The increase in λ value also results in less variability of subsurface flow, as defined in Equation (4). Thus, the predicted mean depth of the water table approaches the surface at the initial stage, and the average saturation deficit obtained from Equation (25) remains around zero. In the model, zero saturation deficit means that the state of the vertical soil profile is completely saturated up to the surface. Any further rainfall after the zero local saturation deficit state contributes directly to surface runoff. Figure 14a demonstrates that the average saturation deficit predicted by the 1000 m DEM resolution TOPMODEL, while retaining the effective parameter values identified at the 50 m DEM resolution, shows negative values throughout the simulation period in Event(1). This results in the complete saturation of the local soil moisture deficit in a large part of the catchment from the very beginning of the simulation. This is why the overestimations in simulated discharge during rainfall duration for B(1), B(2) and B(3) are observed in Figure 13.

As we have discussed, the higher λ value results in less variability of subsurface flow rate given by Equation (4). Figure 14b shows that the subsurface flow $Q_b(t)$ obtained from the 1000 m DEM resolution TOPMODEL is almost constant and relatively low during rainfall hours when compared with the other models. The difference of subsurface flow obtained from the 1000 m DEM resolution TOPMODEL and that from the 50 m DEM resolution TOPMODEL or the downscaled 50 m DEM resolution TOPMODEL is significant. This is the reason for the underestimation of the simulated discharge during hours of no rainfall for B(1), B(2) and B(3) in Figure 13.

The overestimation of the simulated discharge in rainfall duration and underestimation of the simulated discharge in the no-rainfall duration is the reason for the increase in the variance in simulated discharge when using a coarse-resolution DEM. Zhang and Montgomery (1994) and Wolock and Price (1994) have also shown that increasing the coarseness of DEM data resolution tended to decrease the mean depth to water table and increase the peak flow.

TOPMODEL coupled with the downscaling method of the topographic index distribution

TOPMODEL coupled with the downscaling method of the topographic index distribution is then applied to solve the prediction error arising from the discrepancy in scales between the scale at which the model parameters are identified and the scale of model applications. The method proposed enables downscaling of the topographic index from a coarse grid-resolution DEM to a fine grid-resolution DEM. Incorporating the downscaled topographic index in TOPMODEL, we can see that the average saturation deficit simulated is quite similar to average saturation deficit simulated by the 50 m DEM resolution TOPMODEL in Figure 14a. As the results of the scaled topographic index distribution and the scaled average saturation deficit produced by the 1000 m grid resolution DEM shown in Figures 11 and 14a match with the topographic index distribution and average saturation deficit produced by the 50 m grid-resolution DEM, simulated discharge of the downscaled TOPMODEL displayed by C(1), C(2) and C(3) in Figure 13 matches the simulated discharge of the 50 m

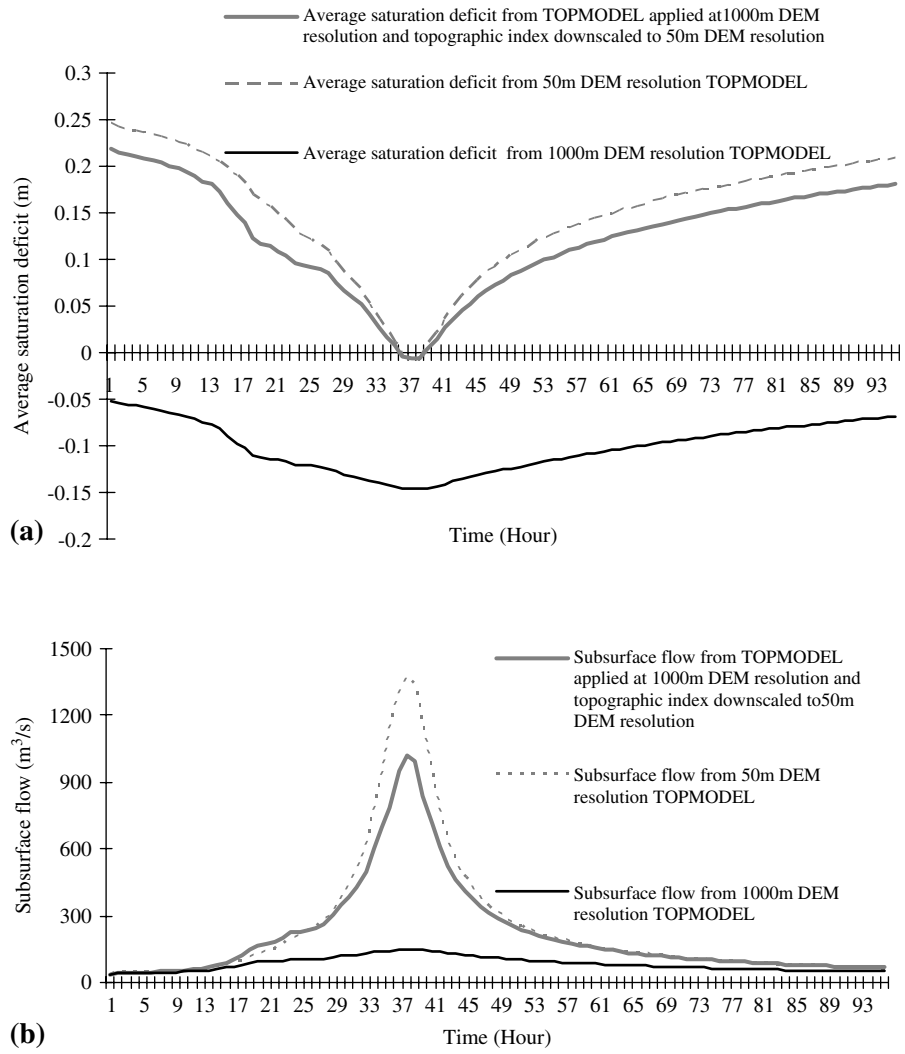

Figure 14. Analysis of average saturation deficit and subsurface flow results of TOPMODEL (with and without coupling the downscaling method of topographic index) applied to the Kamishiiba catchment (210 km^2) for Event(1). (a) Comparison of average saturation deficit obtained from a 50 m DEM resolution TOPMODEL, a 1000 m DEM resolution TOPMODEL and TOPMODEL applied at a 1000 m DEM resolution with scaled topographic index to a 50 m DEM resolution. (b) Comparison of subsurface flow obtained from a 50 m DEM resolution TOPMODEL, a 1000 m DEM resolution TOPMODEL and TOPMODEL applied at a 1000 m DEM resolution with scaled topographic index to a 50 m DEM resolution. In the results of (a) and (b), the applied effective parameters are identified by a 50 m DEM resolution TOPMODEL

DEM resolution TOPMODEL displayed by A(1), A(2) and A(3) in Figure 13. Thus, the Nash efficiencies for C(1), C(2) and C(3) are 92%, 89% and 71% respectively in Figure 13.

An increase in λ, the mean of $\ln(a/\tan\beta)$, caused by using a coarser scale DEM, would be compensated by an increase in calibrated value of T_0, producing similar observed and simulated hydrographs. The parameter value, however, would exceed physically acceptable ranges, leading to the problem of false assumptions that are less restrictive than otherwise thought, as calibration can often compensate for such deficiencies. Table IV shows the DEM resolution dependence of the effective parameter value of T_0 in TOPMODEL. The parameter value of T_0 in Table IV is the calibrated value for each DEM resolution to get the highest Nash efficiency in

Table IV. Scale dependence of effective parameter values in TOPMODEL and downscaling method of topographic index distribution for its solution

DEM resolution (m) parameter	50	500	1000
Calibrated effective parametric value of T_0 (m^2 h^{-1}) for the highest Nash efficiency [%]	6·0 [96·1]	90 [95·4]	200 [95·6]
Nash efficiency (%) at $T_0 = 6{\cdot}0$ m^2 h^{-1}	96·1	70·9	20·5
Nash efficiency (%) with downscaled topographic index to 50 m DEM resolution and using $T_0 = 6{\cdot}0$ m^2 h^{-1}	96·1	94·3	94·1

rainfall Event 1 in the Kamishiiba catchment. In calibrating the effective parameter value at different DEM resolutions, Table IV shows that the T_0 value has to be increased from 6·0 m^2 h^{-1} at a 50 m DEM resolution to 200 m^2 h^{-1} at a 1000 m DEM resolution to obtain the highest Nash efficiency. Ibbitt andWoods (2004) and Franchini *et al*. (1996) point out that such a high soil parameter value may preserve subsurface flow properties in a desirable way, but at the same time could affect the infiltration behaviour, if the vertical and lateral hydraulic conductivities are assumed to be equal in the TOPMODEL framework. Table IV shows the drop in Nash efficiency when the same value of T_0 identified at a 50 m DEM resolution is used for different DEM resolutions. Table IV also demonstrates that the Nash efficiency converges to a maximum Nash efficiency at each of the DEM resolutions when the topographic index is downscaled to a 50 m DEM resolution from the respective DEM resolutions and the same value of T_0 that is identified at a 50 m DEM resolution is used. This proves that TOPMODEL coupled with the downscaling method of topographic index distribution defined by Equation (21) is consistent with observations (observed discharge data), although the scale of the DEM at which the parameters are identified and the scale of the DEM at which the model is applied are dissimilar.

CONCLUSIONS

There is a long tradition in geomorphology of seeking general rules for landscape evolution so as to provide a topographic framework for hydrological, ecologic, or other landscape-based models. Geomorphological features obtained from DEMs are influenced by the resolution of the DEM. In this study we developed a method to downscale the upslope catchment area to solve the effect of DEM resolution on the upslope catchment area. Through analysis of scale laws, the concept of a resolution factor has been developed in this study to account for the effect of scale on upslope catchment area per unit contour length in topographic index, and a fractal method for scaled steepest slope has been developed as an approach to account for the effect of scale on slopes. These are combined to develop the method to downscale the topographic index distribution. The method for downscaling the topographic index represents a scale-invariant function for topographic index distribution and has made possible the utilization of parameter values calibrated using high-resolution DEMs in making predictions with TOPMODEL using coarser resolution DEMs. This study can be extended in analysis of scaling behaviour across catchments through developing a topography-driven regionalization model, at least for regions that are 'homogeneous' in some sense (Pradhan *et al*. 2005). Although assessment of uncertainty has not been conducted as part of this study, it is worth noting that a large part of the uncertainty in hydrological prediction can be reduced if the phenomenon of the uncertainty is understood (Sivapalan *et al*., 2003). It is hoped that the downscaling method can reduce the parametric uncertainty by reducing the feasible parameter value range in grouping of models into functional classes according to similarity of predictions for some variable of interest, as defined by Beven (2000b). It is also hoped that the findings of this study will demonstrate their applicability as a tool to solve a wider range of problems, especially with respect to scale issues, when modelling hydrological processes.

ACKNOWLEDGEMENTS

Special thanks go to Professor K. Beven at the University of Lancaster for his valuable comments on the manuscript. We also thank an anonymous referee and Dr T. Nakaegawa for their valuable advice.

REFERENCES

Abbott MB, Bathurst JC, Cunge JA, O'Connell PE, Rasmussen J. 1986b. An introduction to the European Hydrological System–Système Hydrologique Europeèn, SHE, 2: Structure of a physically-based, distributed modelling system. *Journal of Hydrology* **87**: 61–77.

Ambroise B, Beven K, Freer J. 1996. Towards a generalization of the TOPMODEL concepts: topographic indices of hydrologic similarity. *Water Resources Research* **32**: 2135–2145.

Andrle R, Abrahams AD. 1989. Fractal techniques and the surface roughness of talus slopes. *Earth Surface Processes and Landforms* **14**: 197–209.

Band LE, Moore ID. 1995. Scale: landscape attributes and geographical information systems. *Scale Issues in Hydrological Modelling*, Kalma JD, Sivapalan M (eds). Wiley: Chichester; 159–179.

Beven K. 1986. Runoff production and flood frequency in catchments of order n: an alternative approach. *Scale Problems in Hydrology*, Gupta VK, Rodríguez-Iturbe I, Wood EF (eds). Reidel: Dordrecht; 107–131.

Beven K. 1987. Towards the use of catchment geomorphology in flood frequency predictions. *Earth Surface Processes and Landforms* **12**: 69–82.

Beven K. 1995. Linking parameters across scales: subgrid parameterizations and scale dependent hydrological models. *Scale Issues in Hydrological Modelling*, Kalma JD, Sivapalan M (eds). Wiley: Chichester; 263–281.

Beven KJ. 2000a. *Rainfall-Runoff Modelling.* Wiley: New York.

Beven KJ. 2000b. Uniqueness of place and process representations in hydrological modeling. *Hydrology and Earth System Sciences* **4**: 203–214.

Beven K. 2002. Towards an alternative blueprint for a physically based digitally simulated hydrologic response modelling system. *Hydrological Processes* **16**: 189–206.

Beven KJ, Kirkby MJ. 1979. A physically based, variable contributing area model of basin hydrology. *Hydrological Sciences Bulletin* **24**: 43–69.

Bruneau P, Gascuel-Odoux C, Robin P, Merot Ph, Beven KJ. 1995. Sensitivity to space and time resolution of a hydrological model using digital elevation data. *Hydrological Processes* **9**: 69–82.

Cunge JA. 1969. On the subject of a flood propagation computation method (Muskingum method). *Journal of Hydraulic Research* **7**: 205–230.

Dunne T, Black RD. 1970. An experimental investigation of runoff production in permeable soils. *Water Resources Research* **6**: 478–490.

Franchini M, Wendling J, Obled C, Todini E. 1996. Physical interpretation and sensitivity analysis of the TOPMODEL. *Journal of Hydrology* **175**: 293–338.

Freeze RA, Harlan RL. 1969. Blueprint for a physically based, digitally simulated hydrological response model. *Journal of Hydrology* **9**: 237–258.

Goodchild MF. 2001. Models of scale and scales of modelling. *Modelling Scale in Geographical Information Science*, Tate NJ, Atkinson PM (eds). Wiley: Chichester; 3–10.

Güntner A, Uhlenbrook S, Seibert J, Leibundgut Ch. 1999. Multi-criterial validation of TOPMODEL in a mountainous catchment. *Hydrological Processes* **13**: 1603–1620.

Ibbitt R, Woods R. 2004. Re-scaling the topographic index to improve the representation of physical processes in catchment models. *Journal of Hydrology* **293**: 205–218.

Iorgulescu I, Jordan J-P. 1994. Validation of TOPMODEL on a small Swiss catchment. *Journal of Hydrology* **159**: 255–273.

Jenson SK, Domingue JQ. 1988. Extracting topographic structures from digital elevation data for geographic information systems analysis. *Photogrammetric Engineering and Remote Sensing* **54**: 1593–1600.

Kirkby MJ. 1975. Hydrograph modeling strategies. *Process in Physical and Human Geography*, Peel R, Chisholm M, Haggett P (eds). Heinemann: London; 69–90.

Klinkenberg B, Goodchild MF. 1992. The fractal properties of topography: a comparison of methods. *Earth Surface processes and Landforms* **17**: 217–234.

Leopold LB, Maddock T. 1953. The hydraulic geometry of stream channels and some physiographic implications, *United States, Geological Survey, Professional Papers* **252**.

Mendicino G, Sole A. 1997. The information content theory for the estimation of the topographic index distribution used in TOPMODEL. *Hydrological Processes* **11**: 1099–1114.

O'Loughlin EM. 1986. Prediction of surface saturation zones in natural catchments by topographic analysis. *Water Resources Research* **22**: 794–804.

Pradhan NR, Tachikawa Y, Takara K. 2004. A scale invariance model for spatial downscaling of topographic index in TOPMODEL. *Annual Journal of Hydraulic Engineering, JSCE* **48**: 109–114.

Pradhan NR, Tachikawa Y, Takara K. 2005. Development of a transferable hydrologic modeling in TOPMODEL framework across scale and region. *Annual Journal of Hydraulic Engineering, JSCE* **49**: 217–222.

Quinn P, Beven K, Chevallier P, Planchon O. 1991. The prediction of hillslope flow paths for distributed hydrological modelling using digital terrain models. *Hydrological Processes* **5**: 59–79.

Quinn P, Beven K, Lamb R. 1995. The $\ln(a/\tan\beta)$ index: how to calculate it and how to use it within the TOPMODEL framework. *Hydrological Processes* **9**: 161–182.

Rodriguez-Iturbe I, Rinaldo A. 1997. *Fractal River Basins: Chance and Self-organization*. Cambridge University Press.

Rogers CCM, Beven KJ, Morris EM, Anderson MG. 1985. Sensitivity analysis, calibration and predictive uncertainty of institute of hydrology distributed model. *Journal of Hydrology* **81**: 179–187.

Saulnier G-M, Obled Ch, Beven KJ. 1997. Analytical compensation between DTM grid resolution and effective values of saturated hydraulic conductivity within the TOPMODEL framework. *Hydrological Processes* **11**: 1331–1346.

Sivapalan M, Takeuchi K, Franks SW, Gupta VK, Karambiri H, Lakshmi V, Liang X, McDonnell JJ, Mendiondo EM, O'Connell PE, Oki T, Pomeroy JW, Schertzer D, Uhlenbrook S, Zehe E. 2003. IAHS Decade on Predictions in Ungauged Basins (PUB), 2003–2012: shaping an exciting future for the hydrological sciences. *Hydrological Sciences Journal–Journal des Sciences Hydrologiques* **48**: 857–880.

Wolock DM, Price CV. 1994. Effects of digital elevation model map scale and data resolution on a topography based watershed model. *Water Resources Research* **30**: 3041–3052.

Woods EF, Beven K, Sivapalan M, Band L. 1988. Effects of spatial variability and scale with implication to hydrology modeling. *Journal of Hydrology* **102**: 29–47.

Woods RA, Sivapalan M, Robinson JS. 1997. Modeling the spatial variability of surface runoff using a topographic index. *Water Resources Research* **33**: 1061–1073.

Zhang W, Montgomery DR. 1994. Digital elevation model grid size, landscape representation, and hydrologic simulations. *Water Resources Research* **30**: 1019–1028.

Zhang X, Drake NA, Wainwright J, Mulligan M. 1999. Comparison of slope estimates from low resolution DEMs: scaling issues and a fractal method for their solution. *Earth Surface Processes and Landforms* **24**: 763–779.

